JOURNAL OF SOLID STATE CHEMISTRY 88, 465–475 (1990)

Incommensurate Composite Modulated $Nb_2Zr_{x-2}O_{2x+1}$: $x = 7.1–10.3$

J. G. THOMPSON,*,[1] R. L. WITHERS,* J. SELLAR,† P. J. BARLOW,* AND B. G. HYDE*

*Research School of Chemistry, Australian National University, GPO Box 4, Canberra ACT 2601, Australia; and †ICI (Australia) Operations P/L, Research Group, Newsom Street, Ascot Vale VIC 3032, Australia

Received February 2, 1990; in revised form May 7, 1990

The compound $Nb_2Zr_{x-2}O_{2x+1}$ has been studied by X-ray powder diffraction and transmission electron microscopy. It was previously thought to be an homologous series M_nO_{2n+2} ($n = 2x$, M = metal) but is more correctly described as a Type II, or composite, modulated structure. Reciprocal space is dominated by a conspicuous set of strong matrix reflections G corresponding to the metrically orthorhombic, average metal subcell (A--a, $a_M \simeq 5.1$, $b_M \simeq 4.9$, $c_M \simeq 5.2$ Å). A rather weaker set of incommensurate satellite reflections occur at $G \pm mq$, m being an integer and $q \simeq 1/xa_M^* + b_M^*$. Electron diffraction data, however, show rows of satellite reflections to be slightly canted away from a_M^*, implying that q has a very small incommensurate component in both the b_M^*, and c_M^*, directions of reciprocal space, i.e., the oxygen subcell is triclinic, and only pseudoorthorhombic.

1. Introduction

Zirconia-based ceramics are usually ZrO_2 "stabilized" by the addition of oxides of lower-valence metals, notably CaO, MgO, and Y_2O_3. The resulting anion-deficient phases adopt either the cubic (fluorite-type) or tetragonal ZrO_2 structures. Because of the desirable properties of "stabilized zirconia," various other oxides have been added. The resulting phase relationships of these other ternary systems have been determined and the properties of the compounds they contain have been examined.

At the ZrO_2-rich end of their phase diagrams, $Nb_2O_5 + ZrO_2$ and $Ta_2O_5 + ZrO_2$ exhibit an apparently orthorhombic phase, which may be regarded as a stabilized, anion-excess zirconia. Earlier work on this phase by Roth *et al.* (*1*) indicated that the phase width was $5 \lesssim ZrO_2 : Nb_2O_5 \lesssim 8$. But there were some puzzling aspects to the apparent behavior of this phase.

On the one hand, across the composition range the α-PbO_2-like orthorhombic subcell ($a \simeq 5.1$, $b \simeq 4.9$, $c \simeq 5.2$ Å in our setting) varied little in its dimensions, and yet X-ray diffraction from powders and single crystals showed the presence of an apparent superstructure along the a direction with its magnitude varying greatly as a function of composition. Specimens prepared with simple molar ratios of components (which included all the specimens studied by Roth *et al.* (*1*)) gave correspondingly simple superstructures (e.g., $6ZrO_2 : Nb_2O_5$ gave an $8 \times a$

[1] To whom correspondence should be addressed.

0022-4596/90 $3.00

superstructure). This suggested that a series of superstructures would occur across the composition range.

On the other hand, within the composition range for the orthorhombic phase there was no evidence for two superstructures coexisting, and the solidus appeared to follow a smooth curve. Also, electron diffraction patterns of some specimens required "much longer multiplicities of the subcell than the X-ray data" indicated. At that time (1972) the authors (*1*) stopped short of invoking "a continuous, intimate series of phases with no two-phase regions between them" as an explanation.

There have been two subsequent single crystal structure refinements of compositions with simple molar ratios, $Nb_2Zr_6O_{17}$ (*2*) and $Ta_2Zr_8O_{21}$ (J. Galy, personal communication). These authors treated both structures as simple superstructures of a fluorite-type MO_2 structure. The increase in anion content, as required by the stoichiometry, is accommodated by distortion of the anion array, generating new coordination polyhedra. They proposed that intermediate multiplicities, where the molar ratios were no longer simple or even rational, would be constructed of ordered (or partially ordered) units of neighboring simple superstructures. However, high resolution electron microscope images with the *a*-axis excited are almost invariably perfectly homogeneous and show no evidence for such a superstructure intergrowth model (Fig. 1).

Subsequently, it was suggested that the supernumary anions (with respect to the parent fluorite-type) were accommodated by transforming ribbons of square (4^4) nets of anions to denser (3^6) nets, with subsequent, very minor relaxations in atom positions (*3–5*). This was in accord with the two structures that had been solved.

More recently, the concept of an incommensurately modulated structure has become accepted as necessary and appropriate to explain many previously inexplicable structural anomalies, such as those described by Roth *et al.* (*1*) for the subject compound. The orthorhombic phase $Nb_2Zr_{x-2}O_{2x+1}$: x = 7.1–10.3, described earlier (*1*) as the homologous series M_nO_{2n+2}, $n \equiv 2x$, exhibits all the characteristics of an incommensurately modulated structure, with wave-vector varying continuously with composition. It was therefore decided to update both the description of this region of the phase diagram and the structure of the orthorhombic phase it contains.

2. Experimental

2.1 Synthesis

Many different methods of synthesis of the incommensurately modulated, orthorhombic phase $Nb_2Zr_{x-2}O_{2x+1}$ were attempted. Only one method gave reproducible specimens which were self-consistent in terms of the magnitude of the modulation wave-vector. We will describe here in detail this method. Other methods of synthesis will be described later with reference to why they produced deviant results.

Specimens 1–7 were prepared from ≥ 99.9% Nb_2O_5 and > 99.95% "ZrO_2" (containing 2.57% HfO_2) at compositions with molar ratios of ZrO_2 : Nb_2O_5 of 4.5, 5.0, 5.75, 6.5, 7.25, 8.0, and 8.5, respectively. After intimate mixing of the finely ground powders, specimens were pressed into pellets, heated in air on thin Pt foil supported by alumina at 1350°C for 24 hr, finely ground and repressed, then heated finally at 1350°C for a further 24 hr. The specimens graded from off-white to pale gray in color with increasing Nb_2O_5 content.

2.2 XRD and Electron Diffraction

Specimens were examined by XRD using a Guinier–Hägg camera with monochromated Cu$K\alpha_1$ radiation. An internal standard of Si (NBS No. 640) was used to cali-

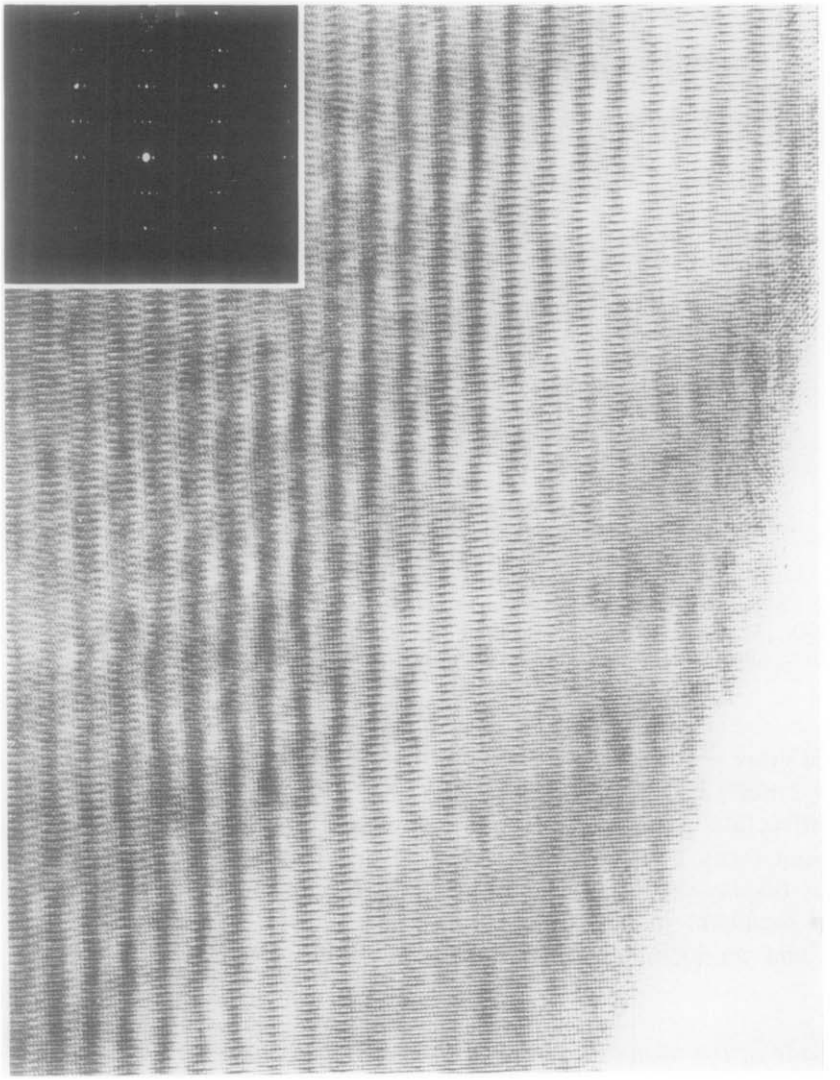

FIG. 1. A typical $[001]_M$ HREM lattice image of an $x \simeq 9.3$ specimen of $Nb_2Zr_{x-2}O_{2x+1}$. The corresponding diffraction pattern is inset (for indexing see Fig. 8d). The regular $9.3/2 \times a_M \simeq 24$ Å fringes running vertically show no evidence for a superstructure intergrowth model.

brate the measurement of XRD films for least-squares refinement of the unit cell dimensions, and magnitude of the modulation wave-vector. The material was further studied on JEOL 100CX, JEOL 200CX, and Philips 430 (with an energy-dispersive X-ray (EDX) spectrometer) transmission electron microscopes.

3. Results and Discussion

3.1 Phase Relationships

The phase relationships are as reported earlier (*1*) except that the incommensurately modulated $Nb_2Zr_{x-2}O_{2x+1}$ phase field is treated as a single phase "solid–solution" (Fig. 2). The end member compositions are

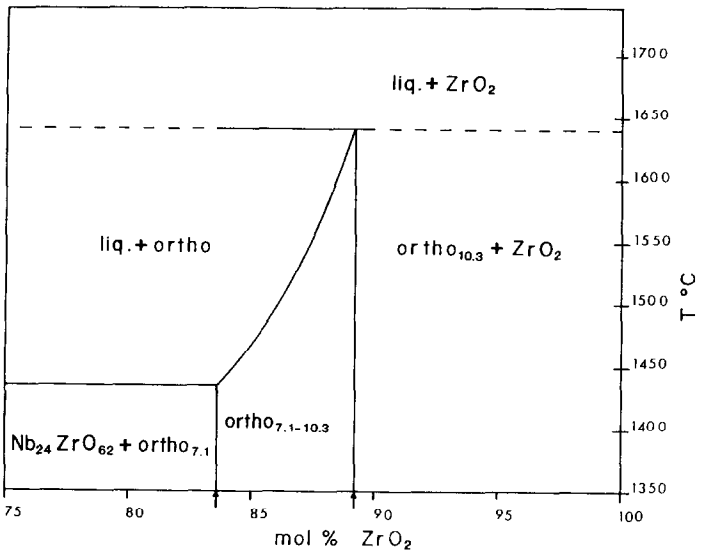

FIG. 2. The ZrO_2-rich end of the phase diagram for the system Nb_2O_5–ZrO_2. From the present work $Nb_2Zr_{x-2}O_{2x+1}$ is treated as a single phase and the limits of its composition are shown as 83.6 and 89.2 mol% ZrO_2, otherwise the data are extracted from Fig. 2 of Roth *et al.* (*1*).

also defined more precisely as occurring at 83.6 and 89.2 mol% ZrO_2 from the XRD and electron diffraction results. Densitometer traces of Specimens 1 and 7 are shown in Fig. 3. They display the diffraction profiles of the end members in equilibrium with $Nb_{24}ZrO_{64}$ and monoclinic ZrO_2, respectively.

3.2 Magnitude of the Modulation Wave-Vector

The magnitude of the modulation wave-vector was determined from both X-ray powder diffraction and electron diffraction patterns. From the Guinier–Hägg films the $220\bar{2}$ and $22\bar{0}2$ satellite reflections (see Section 3.4 for indexing notation) were measured with respect to the 2000 subcell reflection (see Fig. 3). Figure 4 shows a plot of a^*/q_x versus composition for Specimens 1 to 7. As Specimens 1, 2, and 7 were diphasic the nominal compositions have been modified to fit the otherwise linear relationship between molar ratio and the reciprocal of wave-vector magnitude. Electron diffraction patterns from single crystal domains of these same specimens confirmed the measurements from X-ray powder diffraction.

3.3 Unit Cell Dimensions

The unit cell dimensions and cell volume of $Nb_2Zr_{x-2}O_{2x}+1$ are plotted as a function of composition for Specimens 1–7 (Fig. 5). As for Fig. 4 the compositions of Specimens 1, 2, and 7 have been corrected from consideration of the linear relationship between the reciprocal of the wave-vector magnitude and composition. It is notable that while the *a* and *b* dimensions change significantly, by 0.5 and 0.8%, respectively, across the composition range, the cell volume varies by less than 0.3% because *a* and *b* change in opposite senses.

3.4 Electron Diffraction Patterns

Figure 6 shows [100], [010], [$01\bar{1}$], and [001] (subcell) zone-axis Convergent Beam

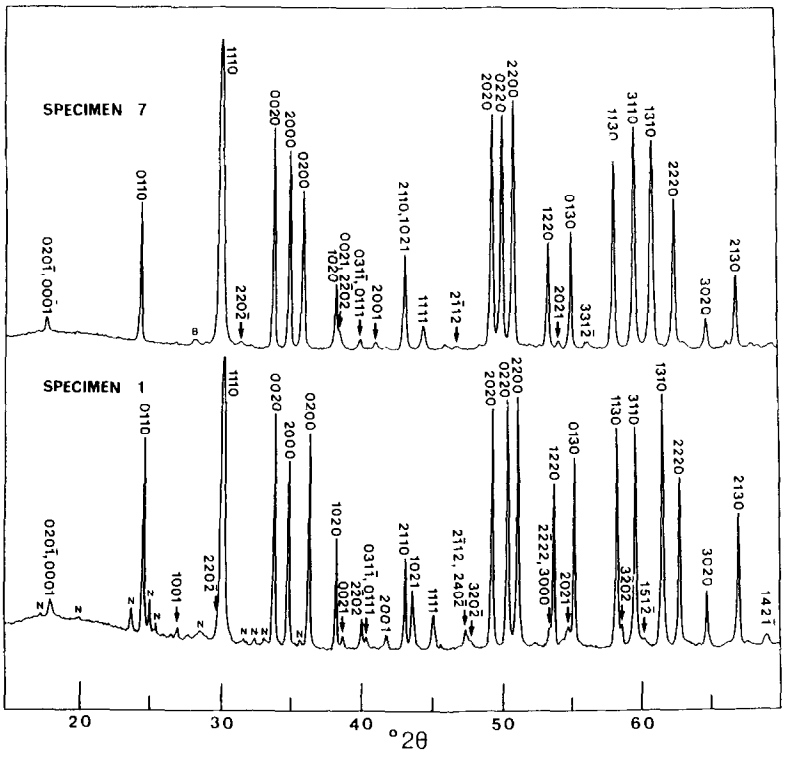

FIG. 3. Densitometer traces from XRD Guinier exposures (λ = 1.5406 Å) of Specimens 1 and 7. Specimen 1 (x = 7.1) is in equilibrium with $Nb_{24}ZrO_{61}$ (N) and Specimen 7 (x = 10.3) with monoclinic ZrO_2, baddelyite (B). A four-index notation (h, k, l, m) has been used to index reflections (see Section 3.4 for explanation). While the subcell reflections (h, k, l, 0) vary little in their position, the satellite reflections often vary significantly, e.g., $22\bar{0}\bar{2}$ and $2\bar{2}02$.

Patterns (CBPs) typical of $Nb_2Zr_{x-2}O_{2x+1}$: x = 7.1–10.3. At first glance, these CBPs appear to be interpretable in terms of a so-called Type I incommensurately modulated structure (*5*). Thus there is always a conspicuous set of strong matrix reflections G (corresponding to an underlying, metrically orthorhombic, average structure; space group *Amma*, $a_M \simeq 5.1$, $b_M \simeq 4.9$, $c_M \simeq 5.2$ Å) accompanied by a rather weaker set of incommensurate satellite reflections at $G \pm mq$, m being an integer and characterized by the primary modulation wave-vector $q \simeq b_M^* + 1/xa_M^*$. A four-index notation (h, k, l, m) = $ha^* + kb^* + lc^* + mq$ can be used to index any given reflection.

It is clear, however, from a Fourier decomposition of the structure refinement of $Nb_2Zr_6O_{17}$ (*2*) and from the nature of the solid-solution field itself that one is really dealing with a Type II, or composite modulated structure (*7, 8*). For an investigation of a composite modulated structure which involves structure determination, see Yamamoto and Nakazawa (*9*). The two components of the composite structure in this case correspond to the averaged metal and oxygen subcells, respectively. Experimentally, this composite character is evident in, for example, the zigzagging of the strongest diffraction intensities along b^* at the [001] (subcell) zone-axis, i.e., for a

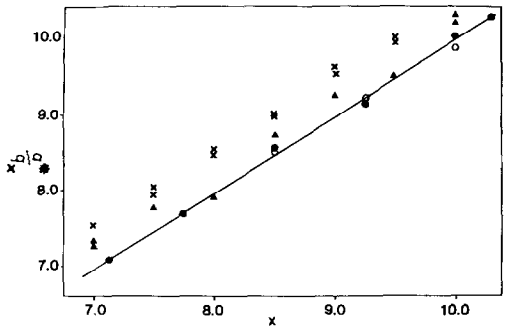

FIG. 4. Plot of a^*/q_x versus composition for Specimens 1–7. As Specimens 1, 2, and 7 were diphasic the nominal compositions have been modified to fit the otherwise linear relationship. ○, data derived from $22\bar{0}\bar{2}$; ●, data from $2\bar{2}02$, from the present work; X, data from Roth *et al.* (*1*); ▲, preliminary results (see Section 3.5).

Type I modulated structure one would not expect $I(\bar{2}20\bar{1}) >> I(\bar{2}001)$ (see Fig. 6d). From a composite modulated structure point of view, however, such intensity discrepancies are quite understandable, e.g., the reflection $(\bar{2}20\bar{1})^*$ in Fig. 6d can also be indexed as $(\bar{1}10)^*$ of the averaged oxygen subcell. It is, in this respect, quite different from its neighboring $(\bar{2}001)^*$ reflection.

Given the continuous smooth variation of $q \simeq b_M^* + 1/xa_M^*$ across the whole solid-solution field (i.e., the lack of any evidence for $1/x$ "locking in" to a rational fraction such as 1/8, 2/17, 1/9, . . .), it is clear that a generally applicable crystallographic description of this phase must be based upon a superspace group approach (*6*) rather than upon conventional crystallographic structure refinement at rational values of $1/x$ (see, for example, the structure refinement of $Nb_2Zr_{x-2}O_{2x+1}: x = 8.0$ (*2*)). Nevertheless such conventional crystal structure refinements, while not properly constrained, are not necessarily incorrect and do provide invaluable insight into the nature of the composite modulated structure. Thus, for $x = 8.0$ (*2*), the reported space group symmetry is *Ima*2 with $a = 40.91$, $b = 4.93$, and $c = 5.27$ Å. Appropriate folding back of this structure solution gives an *Amma*, $a_M = 5.11$, $b_M = 4.93$, $c_M = 5.27$ Å averaged metal subcell and an *Ima*2, $a_O = (x/(2x + 1))a_M = 8/17\, a_M$, $b_O = b_M$, $c_O = c_M$ averaged oxygen subcell (Fig. 7). Interaction of these two, in general, mutually incommensurable components of the composite modulated structure leads to incommensurate modulation of both (*8, 10*). The superspace group implied in the conventional 3-D structure refinement (*2*) (1973) refinement is, in the notation of de Wolff *et al.* (1981) (*6*), $M:Amm2:\bar{1}s\bar{1}$ with characteristic extinction conditions:

$F(hklm) = 0$ unless $k + l = 2n$ (see Fig. 6a) and

$F(hk\bar{l}\bar{k}) = 0$ unless $k = 2n$ (see Fig. 6b).

While we have never detected any break-

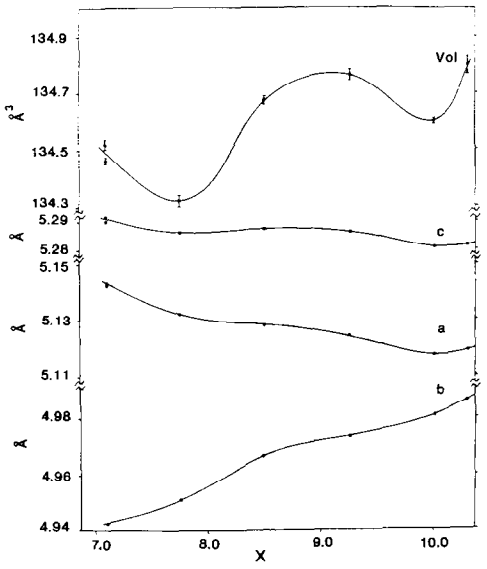

FIG. 5. Plot of unit cell dimensions and cell volume as a function of composition for Specimens 1–7 as in the legend to Fig. 4. The errors in *a*, *b*, and *c* are approximately the symbol dimensions. Because *a* and *b* change in opposite senses, the unit cell volume varies little across the composition range.

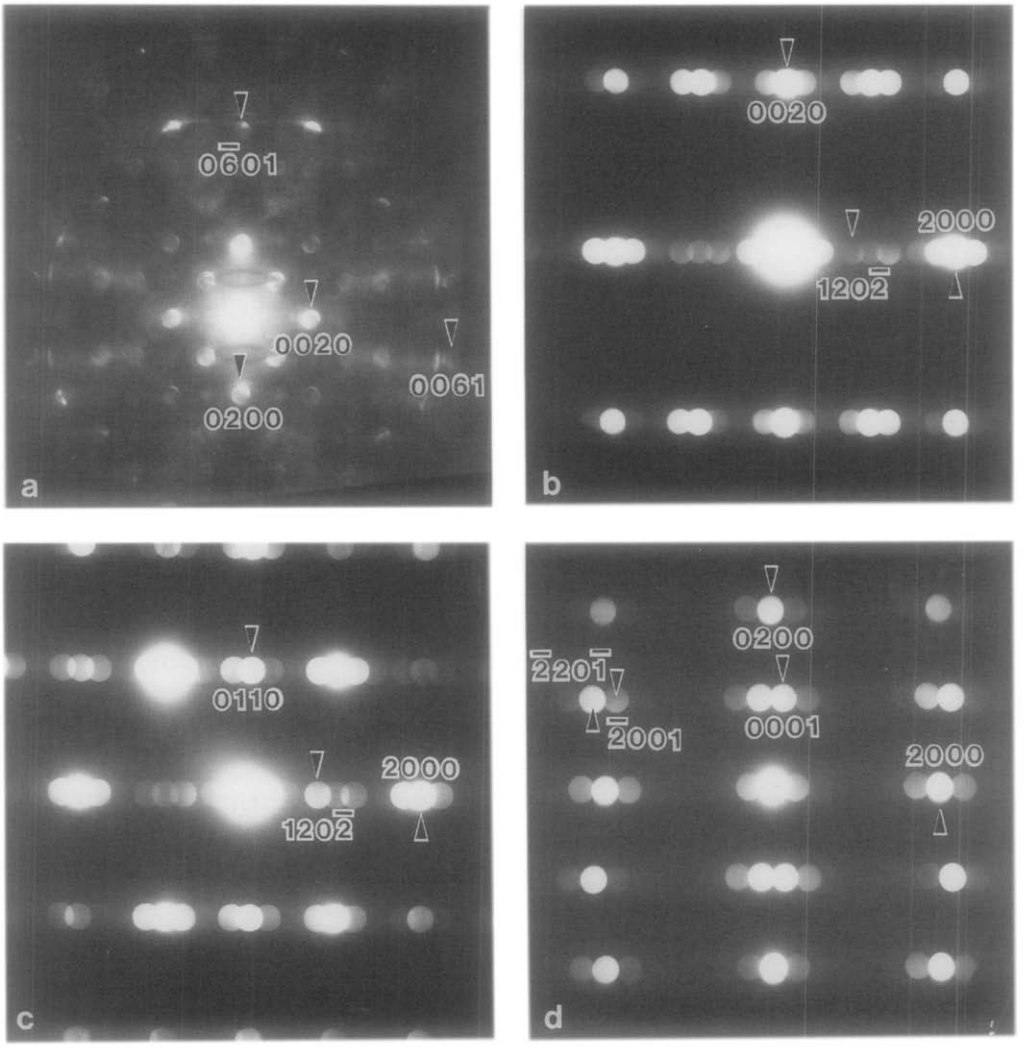

FIG. 6. Shows (a) [100], (b) [010], (c) [01$\bar{1}$], and (d) [001] metal subcell zone axis CBPs typical of $Nb_2Zr_{x-2}O_{2x+1}$: x = 7.1–10.3. The four-index scheme used for labeling reflections is described in the text.

ing of the above extinction conditions, there is nonetheless a major problem with this symmetry description. This can be seen in the [100], [010], [01$\bar{1}$], and [001] (subcell) zone-axis diffraction patterns (SADPs) of Fig. 8. In the latter three SADPs, rows of satellite reflections which should be exactly parallel to a_M^* surround each strong matrix reflection G of the average metal subcell. Close inspection of these SADPs shows that these rows of satellite reflections are always slightly canted away from the exact a_M^* direction, i.e., q is actually given by $1/xa_M^* + (1 - \varepsilon)b_M^* + \delta c_M^*$. That is to say the average oxygen subcell is triclinic and only pseudo-orthorhombic. No splitting of spots is ever observed at the [100] (subcell) zone-axis indicating that the b^* and c^* axes of the average metal and oxygen subcells remain parallel. In conjunction

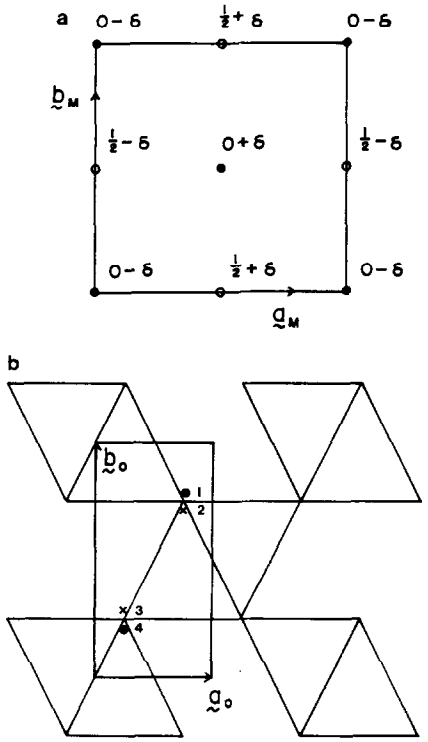

FIG. 7. (a) The *Amma*, $a_M = 5.11$, $b_M = 4.93$, $c_M = 5.27$ Å average metal subcell obtained from the Galy and Roth (*2*) structure refinement of $Nb_2Zr_6O_{17}$. The parameter $\delta = 0.0394$. (b) The *Ima*2, $a_O = (8/17)a_M = 2.405$ Å, $b_O = b_M = 4.93$ Å, $c_O = c_M = 5.27$ Å, average oxygen subcell obtained from the Galy and Roth (*2*) refinement. The fractional co-ordinates of atoms 1, 2, 3, 4 are given by $\frac{3}{4}, \frac{3}{4} + \delta_1, \frac{3}{4} + \delta_2$; $\frac{3}{4}, \frac{3}{4} - \delta_1, \frac{1}{4} + \delta_2$; $\frac{1}{4}, \frac{1}{4} + \delta_1, \frac{1}{4} + \delta_2$; $\frac{1}{4}, \frac{1}{4} - \delta_1, \frac{3}{4} + \delta_2$, respectively. The parameters $\delta_1 = 0.0233$ and $\delta_2 = 0.0081$.

with the slight canting typically observed whenever a_M^* is excited, this observation implies that the b_O and c_O axes of the average oxygen subcell always have small components in the a_M direction. The structural implication of this canting is that the oxygen array is incommensurate with respect to the metal array, not just in the a_M direction, but also in the b_M and c_M directions. However, no triclinicity is ever detectable in the average metal subcell axes.

Wider angle [100] CBPs, however, do show evidence for broken symmetry (Fig. 9). This lowering of symmetry means that the fractional coordinate shifts associated with the incommensurate *mq* modulations are potentially no longer as constrained as the higher symmetry superspace group would imply. Thus a superspace group of $M:Amm2:\bar{1}s\bar{1}$ constrains metal atom shifts associated with odd *m* harmonics to be only along the b_M direction while metal atom shifts associated with even *m* harmonics are constrained to have no b_M component. The lowering of the superspace group symmetry to triclinic removes such constraints. Whether these extra shift components have measurable amplitudes can only be determined by a full X-ray structure refinement based upon a superspace group approach. This, however, is beyond the scope of the present paper.

3.5 Problems with Synthesis

As mentioned earlier, the successful synthesis of satisfactory specimens required many attempts. Initial attempts essentially followed the procedure of Roth *et al.* (*1*). This involved solid-state reaction of mechanically mixed specimens in sealed Pt tubing at temperatures just below the solidus. The specimens were not reproducible with respect to their unit cell dimensions or the magnitude of the modulation wavevector, even when apparently identical procedure was followed. In all cases, however, the specimens appeared to become depleted in Nb_2O_5 relative to the starting composition. This can be seen in Fig. 4 where the a^*/q_x values plot above the line $a^*/q_x = x$. This corresponds to a depletion in Nb_2O_5.

The data of Roth *et al.* (*1*) all plot well above this line, and approximately fit the relationship $a/q_x = (2x + 1)/2$. They initially argued that specimens whose a^*/q_x (multiplicity) fell below this line for a given starting composition "had not been heated long enough and/or at high enough temperatures." However, in a Note Added in Proof these authors reported that specimens pre-

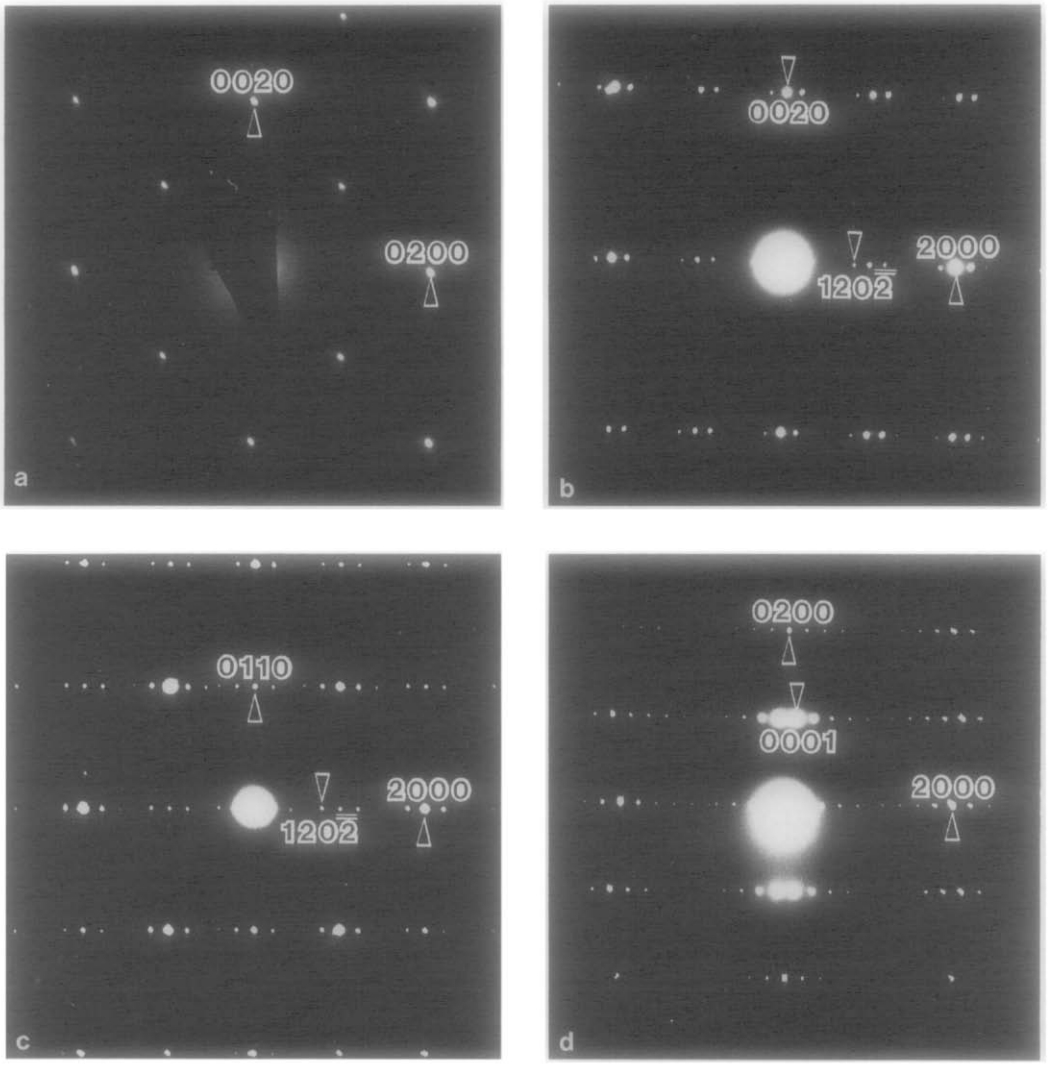

FIG. 8. Shows (a) [100], (b) [010], (c) [$01\bar{1}$], and (d) [001] metal subcell zone axis SADPs typical of $Nb_2Zr_{x-2}O_{2x+1}$: x = 7.1–10.3. Note the slight canting of the satellite reflections away from the a_M^* direction in the latter three SADPs.

pared via the oxidation of the appropriate Nb/Zr alloy obeyed the relationship $a^*/q_x = x$. Our observations for specimens prepared via solid state reaction of the binary oxides confirmed that a significant amount of Nb is lost to Pt and the furnace when specimens are heated at sufficiently high temperatures for even relatively short periods. Energy dispersive X-ray analysis (EDX) of Pt metal which had been used to contain or support such specimens verified this observation. It was the problem of Nb_2O_5 loss to the Pt vessel or support which led us to use minimum reaction times and temperatures with an intermediate remixing, as described above.

3.6 Canting of the Modulation Wave-Vector

The symmetry implications of the canted rows of satellite reflections shown in Fig. 8 prompted us to conduct further experi-

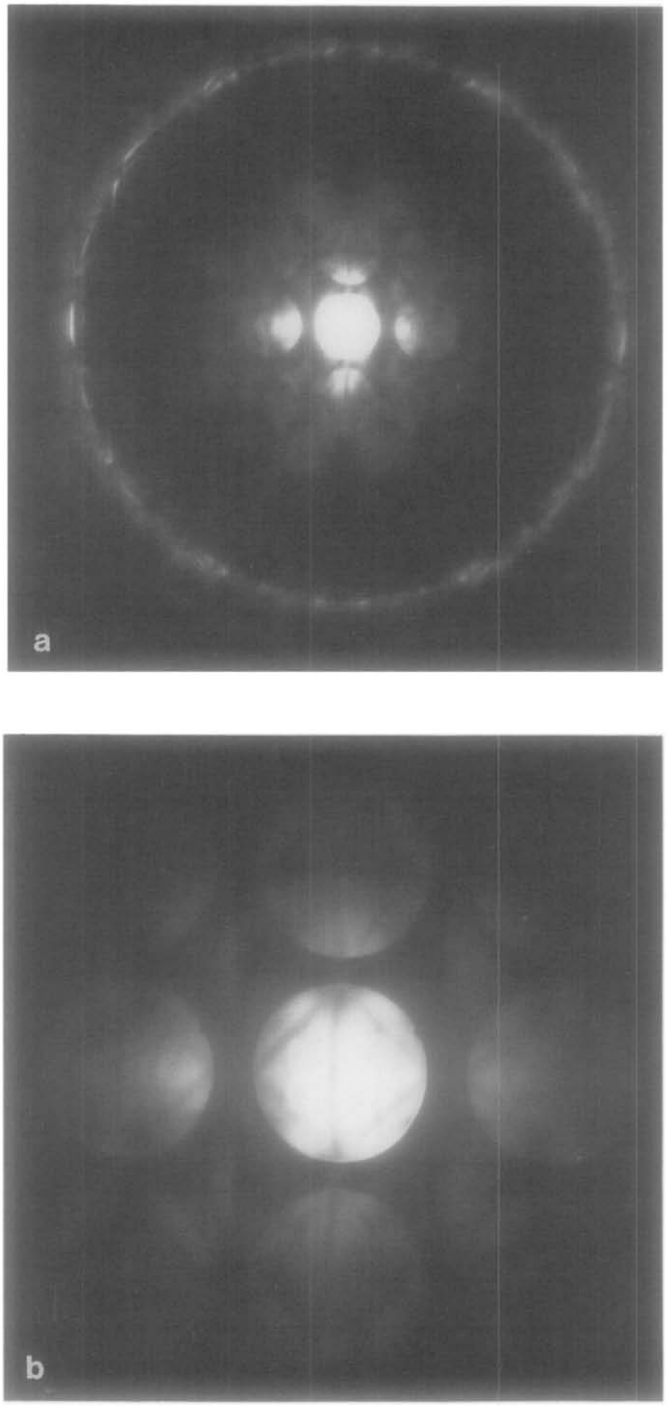

FIG. 9. (a) A wider angle $[100]_M$ zone axis CBP typical of $Nb_2Zr_{x-2}O_{2x+1}$. (b) A magnification of the central portion of the CBP. Note the broken $2mm$ symmetry in both the Zero Order Laue Zone (ZOLZ) and the First OLZ (FOLZ) or satellite HOLZ ring. The b^* axis is horizontal and c^* axis is vertical in both (a) and (b).

ments in order to determine whether there was a simple chemical explanation for the broken symmetry. Specimen 7 was treated under various conditions to attempt to change the magnitude or direction of the modulation wave-vector. These conditions included quenching the specimen from 1600 and 1200°C in sealed Pt tubing, heating the specimen under H_2 at 1000°C for 4 hr (sufficiently reducing conditions to convert Nb_2O_5 to NbO_2), slow cooling in air from 1600°C to room temperature over 48 hr, and cooling in O_2 from 1150°C to room temperature over 16 hr. None of these treatments had any effect on either the X-ray powder diffraction patterns or the electron diffraction patterns. The only observable effects were a slight darkening of the "reduced" and 1600°C quenched specimens and a slight lightening of the slow-cooled specimens. Quite clearly the canting of the rows of satellites was not an artifact of the method of synthesis.

4. Conclusion

A modulated structure approach to $Nb_2Zr_{x-2}O_{2x+1}$: $x = 7.1$–10.3 has two distinct advantages over previous structural descriptions. First, the notion of a series of superstructures, or an homologous series of phases, is not built into the descriptive framework. There is absolutely no requirement, per se, that the average metal and oxygen subcells be mutually commensurable. Second, potential structural degrees of freedom can be readily related to observed diffraction data. Thus modulation of the average structure metal sublattice characterized by modulation wave-vector mq shows up in $G_M + mq$ satellite reflections. The total absence of such satellite reflections for $m > 4$ in the CBPs of Fig. 6 therefore implies that the structural degrees of freedom associated with such modulation wave-vectors must have zero amplitude, i.e., they can be neglected. Such considerations continue to apply even when a superstructure approximation is apparently valid, as for the reported structure refinements of $Nb_2Zr_6O_{17}$ (*2*) and $Ta_2Zr_8O_{21}$ (J. Galy, personal communication), and effectively reduces the number of structural parameters to be determined.

A cursory investigation of $Ta_2Zr_{x-2}O_{2x+1}$ indicates that it is completely analogous to the subject compound, though the exact range of x has yet to be determined. A systematic study of the crystal structure of $M_2Zr_{x-2}O_{2x+1}$ (M = Nb or Ta) across the composition range using a modulated structure approach would help explain the unusual variation in unit cell dimensions with composition, and may provide a crystal chemical explanation for the observed end-member compositions.

Acknowledgments

The authors are indebted to Mr. Gary Williams for his assistance in the preliminary investigations and to Z-tech Pty. Ltd. for the supply of the high-purity ZrO_2 used in this work.

References

1. R. S. Roth, J. L. Waring, W. S. Brower, and H. S. Parker, "Solid State Chemistry: Proc. 5th. Mater. Res. Symp." (R. S. Roth and S. J. Schneider, Eds.), NBS Special Publ. **364,** p. 183 (1972).
2. J. Galy and R. S. Roth, *J. Solid State Chem.* **7,** 277 (1973).
3. B. G. Hyde, A. N. Bagshaw, S. Andersson, and M. O'Keeffe, *Annu. Ref. Mater. Sci.* **4,** 43 (1974).
4. E. Makovicky and B. G. Hyde, *Struct. Bond.* **46,** 101 (1981).
5. B. G. Hyde and S. Andersson, "Inorganic Crystal Structures," Wiley, New York (1989).
6. P. M. de Wolff, T. Janssen, and A. Janner, *Acta Crystallogr., Sect. A* **37,** 625 (1981).
7. A. Janner and T. Janssen, *Acta Crystallogr., Sect. A* **36,** 408 (1980).
8. P. M. de Wolff, *Z. Krystallogr.* **185,** 67 (1988).
9. A. Yamamoto and H. Nakazawa, *Acta Crystallogr., Sect. A* **38,** 79 (1982).
10. P. M. de Wolff, *Acta Crystallogr. Sect. A* **40,** 34 (1984).